



Full Text View

[Volume 30, Issue 2 \(February 2000\)](#)

Journal of Physical Oceanography

Article: pp. 385–401 | [Abstract](#) | [PDF \(919K\)](#)

Examination of the Impact of a Coupled Atmospheric and Ocean Wave System. Part I: Atmospheric Aspects

S. Desjardins and J. Mailhot

Recherche en Prévision Numérique, Atmospheric Environment Service, Dorval, Quebec, Canada

R. Lalbeharry

Recherche en Prévision Numérique, Atmospheric Environment Service, Downsview, Ontario, Canada

(Manuscript received July 27, 1998, in final form April 8, 1999)

DOI: 10.1175/1520-0485(2000)030<0385:EOTIOA>2.0.CO;2

ABSTRACT

To take into account the change of surface roughness length induced by ocean waves, a coupled atmospheric and ocean wave model system is developed. A two-way coupling is done between a mesoscale atmospheric model, MC2, and an oceanic wave model, a regional version of WAM Cycle-4. Two different approaches, based on the wave age of Smith et al. and the wave-induced stress of Janssen, are used to compute a coupling parameter, called the Charnock parameter, expressed as the nondimensional surface roughness length. The coupling between the two models is accomplished by the use of this parameter, which is a function of sea state, instead of the constant value obtained from empirical studies using the well-known Charnock relation.

The coupled atmospheric and ocean wave system was applied to four intense storms in the western Atlantic, to examine the impact of the two-way interaction using real midlatitude storm cases. In Part I, the atmospheric forecasts resulting from this two-way coupling are discussed for these different synoptic cases. The two approaches are evaluated by comparing atmospheric outputs obtained from the coupled and uncoupled systems against buoy observations. The authors conclude that, at least for short-term forecasts, the effects of sea-state-dependent surface roughness on the evolution and synoptic-scale aspects of the storm are rather weak, while small beneficial effects are noted on surface variables.

The most significant changes are a reduction of about 10% of the surface winds associated with enhanced surface roughness lengths in areas of younger and rougher seas. The coupling also modifies the sea surface fluxes by as

Table of Contents:

- [Introduction](#)
- [Coupled atmosphere–ocean](#)
- [Simple analyses of the](#)
- [CASE 1: Superstorm of](#)
- [CASE 2: 7 March 1986](#)
- [CASE 3: The “Bomb”](#)
- [CASE 4: Hurricane Luis](#)
- [Summary and conclusions](#)
- [REFERENCES](#)
- [APPENDIX](#)
- [TABLES](#)
- [FIGURES](#)

Options:

- [Create Reference](#)
- [Email this Article](#)
- [Add to MyArchive](#)
- [Search AMS Glossary](#)

Search CrossRef for:

- [Articles Citing This Article](#)

Search Google Scholar for:

- [S. Desjardins](#)
- [J. Mailhot](#)

much as 50%, but these are not located in the active areas of the storm. Consequently, precipitation only increases slightly and does not affect the storm development. The impact on the ocean wave forecasts is discussed in Part II.

- [R. Lalbeharry](#)

1. Introduction

In recent years several studies have indicated a bidirectional, or two-way, interaction between winds and ocean waves ([Donelan 1982](#); [Janssen 1989, 1991](#); [Chalikov and Makin 1991](#); [Maat et al. 1991](#); [Smith et al. 1992](#)). Based on observations, [Donelan \(1982\)](#) and [Smith et al. \(1992\)](#) concluded that the sea state dependence of momentum transfer at the air–sea interface can be characterized by a single parameter, namely the wave age ξ . This wave age parameter is a good measure of the sea state since it distinguishes the steeper and younger ocean waves ($\xi \sim 5\text{--}10$) from the older and smoother waves ($\xi \sim 25$). [Janssen \(1991\)](#) argued that this was valid only for pure wind sea ($\xi < 25$) and proposed another parameter, the wave-induced stress τ_w , that is also valid for mixed wind sea and swell conditions (the most common occurrence on the ocean). A parameterized version of the theory of [Janssen \(1991\)](#) for the wind–wave interaction was implemented in Cycle-4 of the ocean wave model WAM ([WAMDI Group 1988](#); [Komen et al. 1994](#), hereinafter referred to as WAM4). In this formulation the surface stress (and hence the drag coefficient and the surface roughness length) depends on the sea state. The implication is that in the marine atmospheric boundary layer wind-generated ocean waves may play an important role on the evolution of mesoscale and synoptic-scale weather systems, through the modulation of the surface fluxes of momentum, heat, and moisture.

Variable results have been obtained concerning the role of surface energy fluxes upon extratropical cyclogenesis, ranging from little impact in some cases to substantial effects in other cases, especially at the early stages of storm development ([Uccellini et al. 1987](#); [Mailhot and Chouinard 1989](#); [Kuo et al. 1991](#); [Doyle and Warner 1993](#); [Reed et al. 1993](#); [Huo et al. 1995](#)). [Reed et al. \(1993\)](#) found that the development of the ERICA IOP 5 storm was unusually sensitive to the surface energy fluxes and that, during most of its deepening phase, the storm was characterized by the presence of appreciable upward surface latent heat fluxes in its warm sector. Similar conclusions were reached by [Mailhot and Chouinard \(1989\)](#) for the CASP IOP 14 storm. [Reed et al. \(1993\)](#) noted that this peculiar feature differs strikingly from the flux patterns in other storms that are little or not affected by the surface fluxes and attributed the differences to a storm track more parallel to the Gulf Stream.

Recently, several numerical experiments used coupled ocean wave–atmospheric model systems to investigate the impact of the two-way interaction of winds and waves ([Weber et al. 1993](#); [Janssen 1994](#); [Doyle 1995](#); [Janssen and Viterbo 1996](#); [Lionello et al. 1998](#)). Using a version of WAM coupled with a T21 version of the ECHAM model, [Weber et al. \(1993\)](#) concluded that in a state-of-the-art climate general circulation model, wave growth has no significant impact on the large-scale atmospheric circulation although the interaction between an individual storm and the waves generated by the storm might be strong. It was pointed out ([Janssen 1994](#); [Janssen and Viterbo 1996](#)) that the conclusions of [Weber et al. \(1993\)](#) may be ascribed to the coarse-resolution climate simulations in which extreme events are rare and the strength of storms are not properly reproduced and to an inconsistency in the time-split scheme used, which resulted in surface stress too weak compared to the surface winds. [Janssen \(1994\)](#) and [Janssen and Viterbo \(1996\)](#) coupled a version of WAM with a T63 version of the ECMWF model. They found that the sea state dependence of surface friction resulted in a small, beneficial impact for medium-range forecasts and in a significant impact on the mean state of the atmosphere based on 90-day climate runs.

The studies by [Doyle \(1995\)](#) and [Lionello et al. \(1998\)](#) are both based on coupled simulations of idealized cases of midlatitude cyclones. The high-resolution (30 km) simulations of [Doyle \(1995\)](#) indicated that ocean waves have an impact during the explosive cyclone development by increasing the surface roughness and the surface stress, by decreasing the 10-m wind speeds, and by enhancing the cyclone filling process. The mesoscale structures were also modified locally, leading to enhanced convergence and rainfall. [Lionello et al. \(1998\)](#) noted that the two-way coupling had small effects on the development of the idealized storm and its atmospheric circulation, with only a slight reduction of the storm central pressure. However, the effects were more significant on surface variables, with a decrease of the maximum wave heights and surface wind speeds and an increase of the momentum flux. They argued that their reduced sensitivity to the cyclone intensity and surface fluxes, as compared to those of [Doyle \(1995\)](#), could be attributed to coarser resolution (120 and 60 km) in their study.

In this study we examine the impact of the two-way interaction using real instead of idealized storm cases. Four cases of midlatitude storms have been carefully selected to investigate the short-term impact of coupling on various factors affecting the evolution and structure of these storms: the Superstorm of March 1993, CASP IOP 14 (7 March 1986; also referred to here as the COMPARE I case), the “Bomb” of 4 February 1995, and Hurricane Luis (11 September 1995). In Part I, the atmospheric forecasts resulting from this bidirectional coupling are discussed for these different synoptic cases. The two

approaches (wave age versus wave-induced stress) are evaluated by comparing atmospheric outputs obtained from the coupled and uncoupled systems against buoy observations. The coupled model system is described in [section 2](#), with emphasis on the mesoscale numerical model MC2 and on the coupling and simulation procedures used. In [section 3](#), a simplified analysis of the expected impact of the two-way coupling is presented. [Sections 4 to 7](#) give a synoptic overview and discuss the results for each of the four synoptic cases used in the study.

2. Coupled atmosphere–ocean wave model system

a. Numerical models

The coupled atmosphere–ocean wave model system is composed of an atmospheric model and a wave model exchanging information between them at the end of a given number of model time steps. The coupling is bidirectional since the models influence each other throughout the integration. For this study, the coupled atmosphere–ocean wave model system is constructed with the Mesoscale Compressible Community (hereinafter MC2; [Benoit et al. 1997](#)) meteorological model and a regional version of WAM4. The wave model is described in Part II of this paper ([Lalbeharry et al. 2000](#), hereinafter LMDW). A brief summary of the MC2 model is given in this section. For a more complete description of the MC2 model, see [Benoit et al. \(1997\)](#).

The MC2 is based on the fully elastic nonhydrostatic model of [Tanguay et al. \(1990\)](#). The model solves the Euler equations on a limited-area Cartesian domain of the polar-stereographic projection with time-dependent nesting of the lateral boundary conditions. The model is coupled with the unified RPN physics package that contains a comprehensive set, with several selective options, of parameterization schemes of physical processes ([Benoit et al. 1989](#); [Mailhot et al. 1997, 1998](#)). The main components of the physics package relevant to the processes over the ocean are briefly described in the following paragraph.

The sea surface temperature is kept fixed during the integration. The planetary boundary layer is based on a prognostic equation for turbulent kinetic energy ([Benoit et al. 1989](#)). The stratified surface layer is based on similarity theory. The MC2 model uses a fractional step method for the dynamics together with a fully implicit ($\alpha = 1$) scheme for vertical diffusion, resulting in a scheme that is free of the inconsistency discussed by [Janssen et al. \(1992\)](#). A shallow convection scheme for nonprecipitating clouds is included to give a more realistic description of cloud-topped boundary layers. Condensation processes at resolvable scales account for the formation of stratiform precipitation. An isobaric condensation scheme, which removes moisture when relative humidity exceeds a saturation point, is used with a simplified description of microphysical processes. Deep convective processes are handled with a Kuo-type convective parameterization ([Kuo 1974](#); [Mailhot et al. 1989](#)).

All simulations are done at a resolution of 75 or 50 km with a time step of 600 sec, except for the case of Hurricane Luis, which uses a resolution of 25 km and a time step of 300 s. In the vertical, 30 levels are used extending to the model top at 30 km with a variable distribution to increase the resolution at lower levels (half of them are below 2.5 km and 10 of them in the first kilometer of the atmosphere). [Figure 1](#) shows the horizontal grids used by the coupled system. The WAM ocean wave model is integrated on a latitude–longitude grid on a limited domain enclosed within the larger MC2 domain. The locations of the buoys used for comparisons with the model forecasts are also indicated. The data communication between the models is accomplished through an interface module that includes interpolations on the specific model horizontal grids.

b. Coupling parameter

In an uncoupled system, the surface roughness length over open ocean is obtained from the Charnock relation ([Charnock 1955](#)):

$$z_0 = \frac{\beta_{\text{CH}}}{g} u_*^2, \quad (1)$$

where u_* is the friction velocity, g is the gravitational acceleration, and β_{CH} is the Charnock constant taken as 0.018, a typical value for a mature sea ([Wu 1980](#); [Smith et al. 1992](#)). The Charnock relation makes no reference to sea state and is not a good representation of younger and rougher wind-generated waves.

In the coupled system, β becomes a function of the sea state. The sea state dependence can be expressed in terms of the wave-induced stress ([Janssen 1989](#)) or the wave age ([Smith et al. 1992](#)). Therefore, [\(1\)](#) is reformulated as follows:

where

$$\beta = \beta_{\text{ws}} = 0.01 \sqrt{1 - \left(\frac{\tau_w}{\tau}\right)} \rightarrow \text{wave-induced stress}$$

or

$$\beta = \beta_{\text{WA}} = 0.48(u^*/c_p) \rightarrow \text{wave age.}$$

More details on the two parameterizations of the Charnock parameter are given in LMDW.

Simulations using (1) are used as the control run for each specific case; they will be called the uncoupled runs, referred to as CH (for Charnock relation). Simulations using (2) are two-way coupled runs and will be referred to as WS and WA, for wave-induced stress and wave age, respectively. Note also that, in our study, the roughness lengths computed from either (1) or (2) are used for momentum transfers as well as for heat and moisture transfers at the air–sea interface, although the sea state dependence for heat and moisture transfers is not well supported by observations (e.g., [Smith 1988, 1989](#); [Makin and Masterbroek 1996](#)). In fact, these studies suggest a heat transfer coefficient (the Stanton number) almost independent of wind speed. The assumption of the same sea state dependency for momentum and heat (moisture) transfers possibly leads to an overestimation of the sea state effects on the surface heat and moisture fluxes. The evolution of extratropical marine storms is largely controlled by two competing effects, namely filling of the low by surface drag and deepening by heat and moisture fluxes. In the present study, as discussed in [section 3](#), we limit ourselves to a formulation that is likely to produce the largest sea state impacts on the storm development, using the same sea state dependency for momentum and heat transfers, as a preliminary sensitivity test.

c. Marching procedure

The coupling mechanism has been developed to allow communication between the two models at an arbitrary number of time steps. Let $t_n = T_0 + n\Delta t$, where T_0 is the initial running time, Δt the coupling input time step, and n the actual number of exchanges or couplings done between models. In our case, the coupling interval is $\Delta t = 1800$ s and the MC2 model time step is 600 s so that the coupling takes place every three time steps of MC2. To couple every half hour implies that the sea-state-dependent Charnock parameter remains the same throughout the period. The longer the coupling input time step is, the larger the lag between the sea state and its associated wind field will be. For slow moving or nondeveloping systems this lag is not significant, but for fast moving or developing systems this could be important. In the marching procedure, the wind produced by the MC2 model at t_{n-1} is used as wave model input wind valid at its t_n to allow both models to perform their respective integrations forward in time simultaneously without either one of them waiting on the other.

In the wave model, the Charnock parameter based either on WS or WA is computed by using the most recent wind field input and the previous one, so

$$\beta_n = f(U_{n-2}, U_{n-1}).(3)$$

The MC2 model then uses β provided by the wave model and its own friction velocity u^* to compute the sea-state-dependent roughness length z_0 from (2) so that

$$U_n = f(\beta_{n-1}).(4)$$

Note that due to the two-way coupling, the atmospheric u^* contains information on the sea state as well. The atmospheric model integrates forward in time to produce a new wind field that is passed to the wave model at the next coupling input time step. Each communication between the models implies an exchange of two fields: a *diagnostic 10-m wind field*, from the atmospheric model and the *Charnock parameter* from the ocean wave model. The atmospheric model then uses the new β from the wave model for the next calculation of the surface roughness length. During this time, the waves grow and propagate using the wind given by the atmospheric model.

In the model configurations chosen for this study, the simple addition of the wave model to the atmospheric model requires approximately 45% more CPU time than an uncoupled atmospheric simulation. However, in an operational context, where the wave model is also run twice per day anyway, a coupled atmospheric and wave model system adds overall about 1% CPU time.

Four cases with different synoptic evolutions have been carefully selected to investigate the impact of the coupled atmosphere–ocean wave system on the atmospheric and wave forecasts. [Figure 2](#) shows the 6-hourly observed track together with the evolution of the low pressure center for each case. Three of the cases correspond to rapidly deepening winter storms along the U.S. East Coast, and the fourth case is a hurricane transforming gradually into an extratropical cyclone. Two of the cases have been selected for their generation of extreme sea states and wave heights.

The simulation of each storm case consists of three phases, namely, a spinup phase lasting 48 hours (composed of two 24-h simulations), then a transition phase of 24 hours, and finally the evaluation phase lasting for 36 or 48 hours. The MC2 model is initialized at the start of each phase and after 24 hours into the spinup phase. [Table 1](#) shows the period covered for each case. The coupled model system runs in a control (or uncoupled) CH mode during the spinup phase, which is done only once for each case. Then, the coupled model system runs either in CH, WS, or WA mode during the other phases. The evaluation phase corresponds to the period when the storm is most active and when the impact of the coupling is studied. [Table 2](#) gives the list of numerical experiments for each case in which the bracketed WS indicates that the coupled system in control mode is based on the wave-induced stress parameterization of the surface roughness. Further details on the wave aspects are given in LMDW.

3. Simple analyses of the impact of the coupling

Before proceeding further with the results of control and coupled runs with real cases, it is worth estimating qualitatively the impact of coupling through a simplified scale analysis, for various surface variables, such as the roughness length, the 10-m winds, and the surface fluxes. For the sake of simplicity, neutral static stability conditions are assumed.

Starting with the Charnock relation, one can find that the variation of the roughness length due to the coupling is given by

$$\left(\frac{\Delta z_0}{z_0}\right) = 2\left(\frac{\Delta u_*}{u_*}\right) + \left(\frac{\Delta\beta}{\beta}\right). \quad (5)$$

A detailed derivation is given in the appendix. The ratio $\Delta x/x$ is computed as {coupled x – uncoupled x }/uncoupled x , where uncoupled refers to the control run. [Equation \(5\)](#) indicates that for a same ratio of the sea state term and the velocity term, the friction velocity term contributes to twice the variation of z_0 . However, in most situations, Δu_* due to the coupling will be seen to be very small when compared to the $\Delta\beta$, so the sea state term is the dominant one. A positive $\Delta\beta$ corresponds to an increment of z_0 . When sea state is considered by the wave model to be more mature than the state given by the Charnock constant, a decrease of the roughness length occurs. However in this case, the value of $\Delta\beta$ is often smaller than Δu_* and the first term on the right-hand side can become the dominant one. In this case the variation of the roughness length is proportional to the change in the friction velocity. Intuitively, the coupling with a wave model should increase the friction over the ocean; therefore, in most situations, one expects the friction velocity to increase as well, resulting in an increase of z_0 . Thus, the net result of the coupling, in general, is to increase the surface roughness length since both terms contribute positively.

Applying similar operations to the neutral log wind profile equation and assuming a mean drag coefficient = 2.5×10^{-3} , [Eq. \(A9\)](#) becomes

$$\left(\frac{\Delta u_{10}}{u_{10}}\right) = 0.76\left(\frac{\Delta u_*}{u_*}\right) - 0.12\left(\frac{\Delta\beta}{\beta}\right). \quad (6)$$

[Equation \(6\)](#) shows that a positive increment of β gives a decrease of the wind speed, while an increased friction velocity term increases the wind speed. However, since the second right-hand term in [\(6\)](#) is often the dominant one, the coupling has a general effect of decreasing the wind speed. The situation becomes ambiguous when the Charnock parameter approaches the Charnock constant. In this case, the second-hand term becomes small, and the change on the wind speed is controlled by the sign of the variation of the friction velocity. It will be seen later that the increment of the friction velocity most often follows the sign of the sea state increment. Thus, both terms play against each other and diminish the impact of the coupling on the wind field. One can expect that little change in the wind field will, in return, generate little change on the wave field as well and will modify slightly the Charnock parameter passed to the atmospheric model subsequently.

Finally, for surface heat and moisture fluxes where the surface roughness length for heat and moisture is assumed to be fully sea state dependent (see appendix):

$$F_{\zeta} = \frac{\rho C_{\zeta} - \Delta \zeta}{Pr} (u_z C_D). \quad (7)$$

Assuming neutral conditions and a mean drag coefficient = 2.5×10^{-3} , [Eq. \(A18\)](#) gives

$$\frac{\Delta F_{\zeta}}{F_{\zeta}} = 1.24 \left(\frac{\Delta u_*}{u_*} \right) + 0.12 \left(\frac{\Delta \beta}{\beta} \right). \quad (8)$$

In contrast to the case with the wind speed, in the situation of coupling, both terms act to increase the flux. The contribution of the friction velocity is highly weighted therefore: even though the sea state term is often the dominant one, both terms can sometimes contribute in a proportion more or less equivalent to the variation of the flux.

To get a rough idea of the variations of the surface parameters, let us consider an example. With a 20 m s^{-1} flow, a realistic representation of the roughness of the youngest waves can be about three times the Charnock constant ($\beta = 3 \times \text{CH}$). Friction velocity reaches values of about unity ($u_* = 1 \text{ m s}^{-1}$) and its variation can be about one tenth of this value ($\Delta u_* = 0.1 \text{ m s}^{-1}$). Therefore, from [\(5\)](#) the contribution of the sea state term is about 200%, while the friction velocity term contributes to only 20% for a total increase of 220% in the surface roughness length. An initial $z_0 = 2 \times 10^{-3} \text{ m}$ would then increase to $6.4 \times 10^{-3} \text{ m}$. For the variation of the wind speed given by [\(6\)](#), the sea state term decreases the wind speed by about 24%, while the friction velocity variation produces a wind speed increment of about 8%. Thus, the initial wind speed of 20 m s^{-1} would decrease by about 16% of its initial value, so the coupled winds would be 17 m s^{-1} . Finally, the total increment for the fluxes would be about 36%, corresponding to a contribution of 24% from the sea state term and 12% from the friction velocity term. The use of more common parameterizations based on field data (e.g., [Makin and Mastenbroek 1996](#)), such as a constant thermal roughness length [[\(A15\)](#) in the appendix], result in an increase of only 10%, and by a decrease of about 15% while using a constant Stanton number [[\(A13\)](#) in the appendix].




Note that these simple relations apply only to neutral conditions. Moreover, the calculations used a mean drag coefficient representative of the peak wind events. As a sensitivity test, if the mean drag coefficient is reduced by a factor of 2 in [Eqs. \(6\)](#) and [\(8\)](#), the contribution of the sea state term is altered by 30%, while the contribution of the friction velocity varies by more or less 1%.

4. CASE 1: Superstorm of March 1993

a. Synoptic overview

The Superstorm of March 1993 ([Kocin et al. 1995](#); [Huo et al. 1995](#); [Desjardins et al. 1999](#)) is characterized by very strong winds and an extreme sea state. At 0000 UTC 13 March 1993, a strong low pressure system with a central pressure of 984 hPa ([Kocin et al. 1995](#)) was located in the Gulf of Mexico. It intensified rapidly to reach a central value of 963 hPa at 0000 UTC 14 March over the state of Delaware. Afterwards, it began to fill slowly to reach a central pressure of 968 hPa over Anticosti Island at 0000 UTC 15 March. During the period, southerly winds of $10\text{--}25 \text{ m s}^{-1}$ over the ocean gradually shifted to westerlies of $15\text{--}30 \text{ m s}^{-1}$ and generated significant wave heights up to 15 m (maximum wave heights of 30 m were recorded). [Huo et al. \(1995\)](#) showed that the rapid deepening of the superstorm was strongly coupled with latent heat release. The development of a low-level jet (LLJ), coupled with sensible and latent heat fluxes from the ocean, played an important role in transporting warm and moist air from the boundary layer into the frontal zone, especially during the explosive deepening phase. They also found that the upper-level jet-streak-induced circulations played a crucial role in the cyclogenesis in establishing a dynamic link by inducing a southerly flow component (the LLJ) at low levels. The reader is referred to [Kocin et al. \(1995\)](#) and [Huo et al. \(1995\)](#) for a more complete description of the storm and to [Cardone et al. \(1996\)](#) for a better description of its surface wind field. Note that the evaluation period corresponds to the period where the storm stopped deepening and began to fill slowly.

b. Results

[Figure 3](#)  shows the surface roughness length computed from [\(2\)](#) using WS ([Fig. 3a](#) ) and WA ([Fig. 3b](#) ) superimposed with the CH run. Both coupled runs generate roughness length fields with patterns similar to the “control” run but more intense by about three times or more. Also, the WS run results in larger values of z_0 than does the WA run, especially over the eastern part of the region.

The increase in the roughness length has a direct impact on the wind field, as shown in [Fig. 4](#). Both WS and WA couplings generate a similar wind field pattern with decreased wind speeds over most of the domain compared with the CH run. The wind speed differences between the CH run and WS are slightly larger than those of WA. The southerly jet (east of the cold front) is decreased by about 10% in both coupled simulations. The WS run shows a larger impact with respect to changes in the wind direction (near the warm front) located south of Newfoundland. Both coupled simulations react similarly in the strong southwesterlies behind the cold front, where the wind speed is reduced by about 10%.

[Figure 5](#) shows a comparison of the wind speed between buoy observations and numerical values cubically interpolated at the buoy locations. Canadian buoys report winds as a 10-min vector average, and maximum wind speeds are extracted from the highest running 8-s maxima ([Skey et al. 1995](#)). Following [Smith \(1981\)](#), 5-m observed wind speeds were converted to a height of 10 m. This conversion resulted in little change to the buoy wind speed observations. (It is worth noting that there is an ongoing debate in the marine forecast and wave modeling community concerning buoy measurements under rough and extreme sea state conditions.) There has been much speculation and some observational evidence ([Pond 1968](#); [Skey et al. 1995](#); [Skey et al. 1998](#)) that wind speed measurements reported by buoys tend to be lower than the actual wind speed in high sea conditions. Several possible problems with the buoys have been proposed to explain this, such as sheltering of the buoy anemometers by the high waves, extreme buoy motion, and data processing (averaging period and time). Therefore, it will be assumed in the present study that an acceptable simulation of the wind speed is obtained when the numerical values lie in the range between the observed average and maximum wind speeds.

[Figures 5a and 5b](#) show the 10-m level wind speeds for the East Scotian Slope (buoy 44137) and Banquereau (buoy 44138) buoys, respectively. [Figure 5b](#) indicates that all model simulations overestimate the wind speed in the peak wind event (0000–1200 UTC 14 March 1993). The model wind speed lies between the maximum and the mean observed wind speed at buoy 44137 ([Fig. 5a](#)), while model wind speeds are generally higher than the observed ones at other buoy locations, for example [Fig. 5b](#). The CH run overestimates the wind speed the most. Both coupled runs slightly decrease the wind, especially in the peak wind event. Consistent with [Fig. 4](#), WS decreases the wind speed more than WA. At buoy 44138, the coupling has less impact. Possible reasons for this are that 1) winds are weaker and 2) the difference between uncoupled and coupled z_0 is between 3 and 5 mm (not shown here), while at buoy 44137 it lies between 6 and 9 mm (see [Fig. 6a](#)).

Time series of the z_0 and u^* from the different simulations are shown in [Fig. 6](#). Note, first, that the unrealistic discontinuity at 0000 UTC 14 March is caused by the passage from the transition phase to the evaluation period where the model uses the Charnock constant in the first time steps. Since both coupled runs produce Charnock parameter values that adjust to the Charnock constant, this confirms the representativeness of this constant as a typical value for a mean sea state. The largest z_0 difference between coupled and control runs occurs during the peak wind event and explains the largest impact of the coupling on the wind field at this time. The WS run generates a roughness length larger than the WA by about 50% and both coupled runs dominate by a factor of 4–5 the roughness from the uncoupled run. In agreement with [Fig. 3](#) from LMDW, younger waves are present during this period.

As shown in [Fig. 6b](#), most of the change in the surface roughness length is produced by the change in the Charnock parameter since the change in friction velocity is only about 8%. According to (5) in [section 3](#), the contribution of the sea state term, at the peak wind period, is about 204% since the total increase of the roughness length is about 220% with respect to the uncoupled value. This is caused by a Charnock parameter of 0.05 in the region of rougher sea (see [Fig. 3](#) in LMDW). If these percentages are applied in (6), they give a decrease of the wind speed of about 18%, while the actual value is more around 10%. The difference could be due to the fact that (6) has been derived for neutral conditions.

Referring to (5) and (6) and by looking at [Figs. 5a](#) and [6a](#) after 1200 UTC 14 March, one can understand why the coupling does not have a strong impact on the wind, despite a wind speed of 20 m s^{-1} . Around 1500 UTC, while the friction velocity term contributes to about 10% ($2 \times 5\%$) of the 55% of the increase of the roughness length, the sea state term contributes to about 45% corresponding to $\beta \approx 0.025$. However, when these percentages are put in the wind speed variation [equation \(6\)](#), they give a variation of about 1.5% of the wind speed, which is the case between 1200 and 1800 UTC 14 March. After this period, the friction velocity term is the dominant one and thus explains most of the decrease in the wind speed.

In summary, the impact of the coupling for the Superstorm of March 1993 is to decrease the southerlies ahead of the cold front by about 10% caused by the increased friction due to the presence of younger and rougher seas. When compared to observations, this slight decrease is beneficial since the model overestimates the surface wind speed. Most of the change in the roughness length is generated by the change in the Charnock parameter, with a smaller impact on the friction velocity. However, behind the cold front (after 1200 UTC 14 March at buoy 44137), the rapid decrease of the Charnock parameter to converge to the Charnock constant indicates the presence of a more mature sea. In this situation, the change in the wind speed becomes independent of the sea state and is controlled by the friction velocity due to the coupling.

Although tests were done with the other cases using both WS and WA couplings, only results using WS will be presented in the rest of the paper since WS generates the strongest response. It should be noted, however, that the WA generally produces a better agreement between the wind field and its surface roughness length than WS. This is due to the fact that WA uses mostly wind waves in its calculation, while WS integrates as well the sea swell.

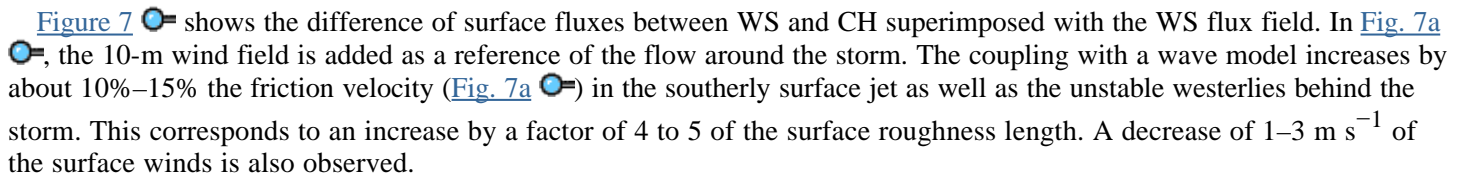
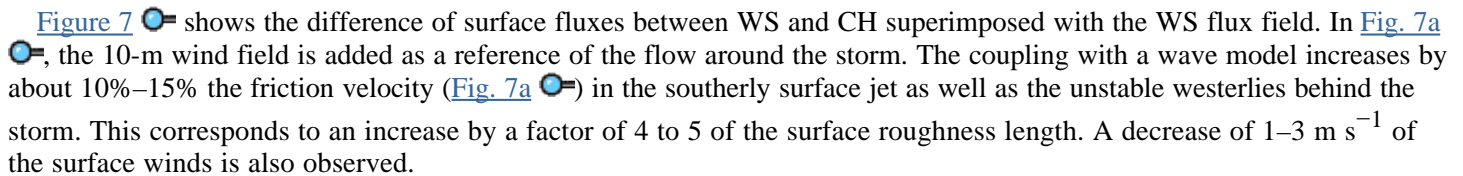
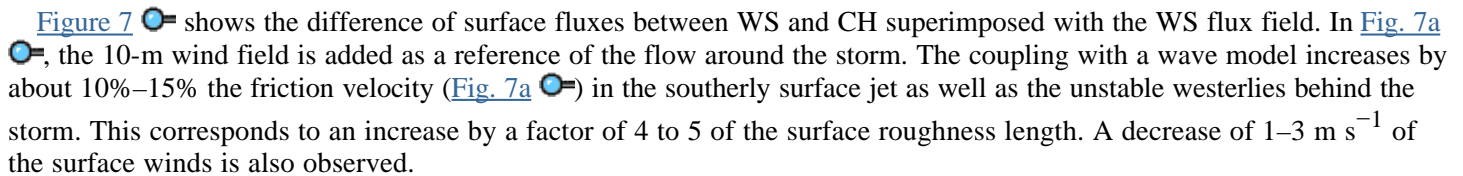
5. CASE 2: 7 March 1986

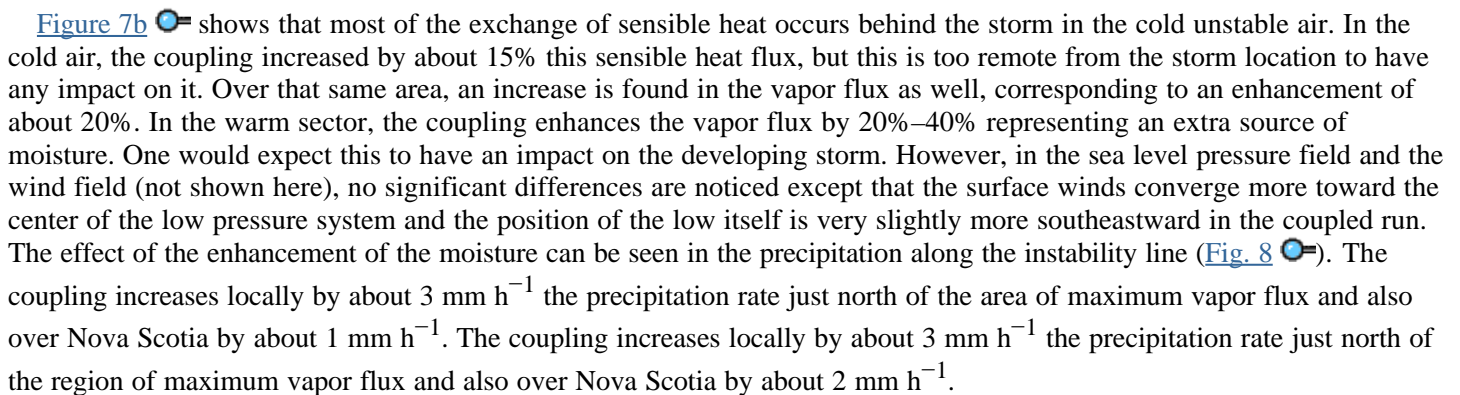
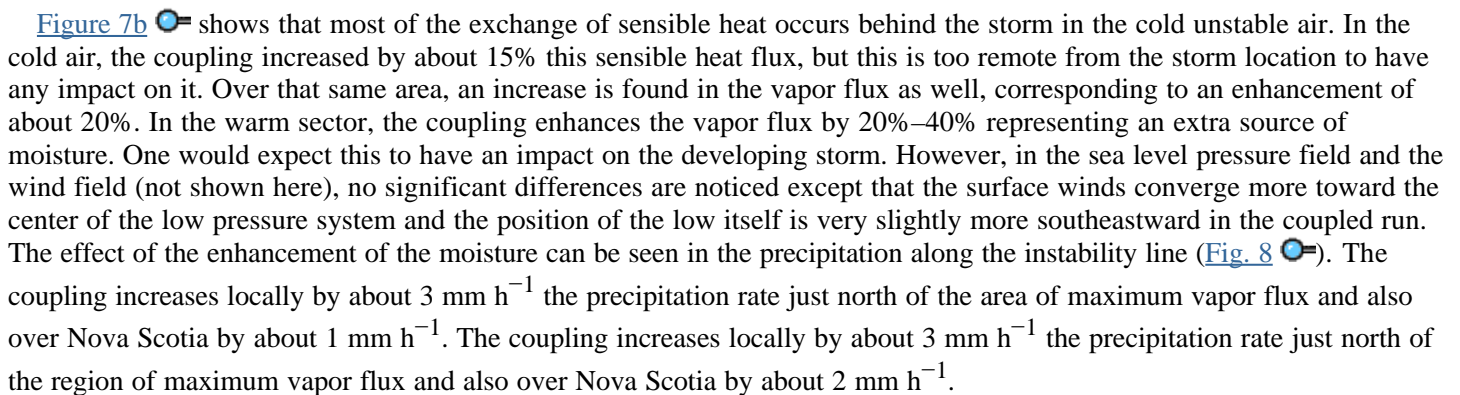
a. Synoptic overview

The next case is the COMPARE I case (Comparison of Mesoscale Prediction and Research Experiments; [Chouinard et al. 1994](#)) that occurred on 6–8 March 1986. At 0000 UTC 7 March 1986, a primary cyclone with a center of 992 hPa was present over Lake Erie. At this time, a secondary low pressure center reaching 996 hPa was developing off the coast just south of Long Island in the trough extending from the primary low. In the next 12 hours, this coastal cyclone explosively deepened at a rate of $18 \text{ hPa} (12 \text{ h})^{-1}$ between 0600 and 1200 UTC 7 March, while the former cyclone became a trailing trough of the major storm. By 1200 UTC 7 March, the central pressure reached 977 hPa as the storm was approaching the southwestern tip of Nova Scotia. The storm then continued to track northeastward throughout the Gulf of St. Lawrence where it gradually occluded.

Various studies ([Mailhot and Chouinard 1989](#); [Yau and Jean 1989](#); [Chouinard et al. 1994](#)) showed that very intense surface fluxes of sensible and latent heat were present in the warm sector of the wave just east of the disturbance. Moreover, a low-level jet with high moisture content was also present in the warm sector just ahead of the cold front. Numerical experiments indicated that the coupling of the intense southerly LLJ with the strong sea surface fluxes, especially evaporation from the ocean, was a critical factor for the rapid deepening of the storm by providing a large portion of the moisture necessary for condensation processes during the rapidly deepening phase. Since the development of this storm has been identified to be sensitive to sea surface fluxes, it is a good case to assess the impact of the coupling on the storm development through the modulation of sea surface fluxes.

b. Results

[Figure 7](#)  shows the difference of surface fluxes between WS and CH superimposed with the WS flux field. In [Fig. 7a](#) , the 10-m wind field is added as a reference of the flow around the storm. The coupling with a wave model increases by about 10%–15% the friction velocity ([Fig. 7a](#) ) in the southerly surface jet as well as the unstable westerlies behind the storm. This corresponds to an increase by a factor of 4 to 5 of the surface roughness length. A decrease of $1\text{--}3 \text{ m s}^{-1}$ of the surface winds is also observed.

[Figure 7b](#)  shows that most of the exchange of sensible heat occurs behind the storm in the cold unstable air. In the cold air, the coupling increased by about 15% this sensible heat flux, but this is too remote from the storm location to have any impact on it. Over that same area, an increase is found in the vapor flux as well, corresponding to an enhancement of about 20%. In the warm sector, the coupling enhances the vapor flux by 20%–40% representing an extra source of moisture. One would expect this to have an impact on the developing storm. However, in the sea level pressure field and the wind field (not shown here), no significant differences are noticed except that the surface winds converge more toward the center of the low pressure system and the position of the low itself is very slightly more southeastward in the coupled run. The effect of the enhancement of the moisture can be seen in the precipitation along the instability line ([Fig. 8](#) ). The coupling increases locally by about 3 mm h^{-1} the precipitation rate just north of the area of maximum vapor flux and also over Nova Scotia by about 1 mm h^{-1} . The coupling increases locally by about 3 mm h^{-1} the precipitation rate just north of the region of maximum vapor flux and also over Nova Scotia by about 2 mm h^{-1} .

In summary, the impact of the coupling on the developing cyclone on 7 March 1986 is very little for the synoptic aspects, but it changes by more than 15% the sea surface fluxes. Most of the change is seen in the wind field where the increased surface friction decreases the surface wind speed and changes the direction of the wind with slightly more cross-isobar flow. Precipitation is locally enhanced where significant changes are observed in the sea fluxes.

6. CASE 3: The “Bomb” of 4 February 1995

a. Synoptic overview

This case is an explosive redevelopment along the East Coast and is listed as one of the interesting cases in the northeastern snowstorm inventory by [Zika and Kocin \(1998\)](#). At 0000 UTC 4 February 1995, a 1003-hPa surface low pressure system over Kentucky, accompanied by a surface wave over western North Carolina and a strong baroclinic zone, was supported by a major upper trough over the eastern part of the continent. As the surface system approached the coast,

a LLJ developed over the Gulf Stream area, pumping moisture from the Gulf Stream and from the Gulf of Mexico. In the next 12 hours, cold advection increased behind the system and strengthened the surface cold front. At 1200 UTC 4 February 1995, the satellite imagery revealed unstable conditions ahead of the front and along the Gulf Stream as a line of convective clouds developed. These conditions favored the development of a wave over North Carolina instead of the primary low, and at the same time a low pressure center at 993 hPa over Chesapeake Bay had formed. In the next 18 hours, this cyclone tracked along the coast and explosively deepened at an average rate of $18 \text{ hPa} (12 \text{ h})^{-1}$. After 0600 UTC 5 February, slight deepening continued for 12 hours as the cyclone moved onshore and crossed New Brunswick.

This case was selected as a sensitivity test to assess the influence of the coupling on the surface jet ahead of the system. A number of dynamic forcing mechanisms have been discussed in relation with coastal LLJ formation and evolution, such as strong geostrophic forcing associated with shallow coastal baroclinicity, surface sensible heat fluxes and condensation latent heat release, and mass/momentum adjustments associated with upper-level jet streaks (e.g., [Uccellini et al. 1987](#); [Lapenta and Seaman 1992](#); [Doyle and Warner 1993](#)). As shown by [Uccellini et al. \(1987\)](#), the presence of a very strong LLJ in the warm sector brings moisture and warm air into the core of the cyclone and is often a key factor for the development of this type of storm. Since the LLJ is seen as an important mechanism in cyclogenesis, a significant change in this jet caused by a coupling with a wave model could possibly modify the behavior of the storm itself. While coastal LLJs are usually confined to a shallow vertical extension in the marine atmospheric boundary layer, LLJs associated with upper-level forcings may extend considerably higher up above the boundary layer ([Uccellini et al. 1987](#); [Lapenta and Seaman 1992](#)). The present case has a well-defined jet core near the surface with a vertical extension up to 700 hPa.

b. Results

Comparison of CH and WS revealed little impact of the coupling on the synoptic system (not shown). As a sensitivity test and to put more emphasis on the region of the jet, another run called 5WS was done where [Eq. \(2\)](#) was multiplied by a factor of 5 when β received from the wave model exceeded two times the Charnock constant. Note that this multiplication factor is only applied in the atmospheric model. The impact on the wave field is discussed in more details in LMDW.

[Figure 9](#) shows a comparison of the 10-m wind speed between buoy observations and numerical values at the East Hatteras (41001) and Gulf of Maine (44005) buoy locations (the same corrections as in [Fig. 5](#) were applied to the 5-m observed wind speed). The East Hatteras buoy represents the early stage of the surface jet, while the Gulf of Maine buoy is representative of the stage where the storm is rapidly deepening. The early stage of the storm ([Fig. 9a](#)) is quite well forecast by the model. The model wind speed at the East Hatteras buoy location agrees closely with the average observed wind speed, except after 0900 UTC 5 February. The rapid deepening stage ([Fig. 9b](#)) indicates a delay by a few hours in the passage of the model LLJ compared to the observations. During the peak wind event (around 0000 UTC 5 February), the model wind speed at the Gulf of Maine buoy location agrees more with the maximum observed wind speed than with the average wind. Therefore, the wind speed at the Gulf of Maine buoy is overestimated, leading to a corresponding overestimation in the wave heights (see [Fig. 5](#) in LMDW). The rapid decrease of the wind speed at the East Hatteras buoy (around 1800 UTC 4 February) is also well simulated. At the Gulf of Maine buoy (44005), the rapid decrease of the wind speed (after 0000 UTC 5 February) is due to the proximity of the low center and may suggest also an error in the location and the central pressure of the storm.

The WS coupling has more impact at the northern buoy since it reduces the value of the CH peak winds by about 10%, while at the southern buoy differences between the control run and the coupled wind speed are negligible. The artificial enhancement (by a factor of 5) of β applies between 1000 and 1800 UTC 4 February 1995 for the East Hatteras buoy and between 1600 UTC 4 February and 0400 UTC 5 February for the Gulf of Maine buoy. The effect of this enhancement is to decrease by about 25% the wind speed at the Gulf of Maine buoy and only 10% at the East Hatteras buoy. It is noteworthy that the amount of decrease of wind speed at the Gulf of Maine buoy is about the same found in the core of the WS surface jet ($\sim 25 \text{ m s}^{-1}$). The overestimation of the wind speed at the buoy 44005 location and that the wind increases more gradually here than at buoy 41001 (the rapid increase of the wind occurs during 18 hours at 44005 while at 41001 the peak wind is attained after 12 hours) can explain the stronger impact of the coupling at the northern buoy. These conditions give higher friction velocity and Charnock parameter values for a longer interval.

[Figure 10](#) shows a superposition of pressure patterns with their wind field of the two coupled runs. Darker lines represent the output from the 5WS run, while the thinner wind barbs and the dashed lines are for WS. Very little change occurs in the intensity (1 hPa deeper) and position of the storm between the two coupled runs. The main change is found in the pressure gradient where a general slackening is noticed with 5WS. Another feature is the marked surface trough caused by cold air advection behind the system. This trough has a more pronounced curvature in the 5WS version. This results in a stronger shifting of the wind and therefore generates more convergence. This noticeable change of the isobaric curvature at this location is caused by the young and rougher waves generated by the wind blowing offshore. In 5WS, the sea surface fluxes are increased by 40%–80% when compared to WS. A cross section (not shown here) through the surface jet streak demonstrates that this enhancement of the surface fluxes slightly increases the moisture up to 850 hPa and warms up by about 1°C or less the whole atmospheric column up to the tropopause.

A comparison of the vertical profile of the wind speed at Portland, Maine (Fig. 11), indicates significant errors in the simulations. While the observed maximum jet is around 750 hPa, the simulations develop it around 650 hPa with a vertical extension much larger than observed. The WS run very slightly decreased the wind speed throughout the entire column. The 5WS run emphasizes more this decrease but indicates as well that the coupling with a wave model, in general, has a rather small impact on the vertical structure of the wind and on the layers aloft.

In summary, multiplying the Charnock parameter by a factor of 5 certainly has a strong impact on the surface wind speed. It greatly modifies the sea fluxes but, in general, does not noticeably change the behavior of the storm. Examination at upper levels reveals that the “boosted” Charnock parameter has a rather modest impact in the mid and high levels, especially when one considers the highly exaggerated roughness length. This emphasizes again that, overall, the coupling does not seem to have a strong impact on the synoptic evolution of the storm, except for surface variables.

7. CASE 4: Hurricane Luis of September 1995

a. Synoptic overview

The period of interest occurs when Hurricane Luis tracked rapidly northeastward at a speed of about 35 knots to reach Newfoundland by 0600 UTC 11 September 1995. During this transition period, Hurricane Luis was gradually transforming into an extratropical cyclone after being captured by the extratropical upper-level circulation. Our initial analyses of the hurricane clearly suffered from a lack of data in its vicinity, as the intensity and the vertical structure of the hurricane were poorly represented at the initial time. Nevertheless, despite that the observed behavior of the hurricane and its surface features could hardly be well simulated, the case was retained as a sensitivity test to assess the impact of the coupling on a mainly convectively driven system. By modifying the surface roughness length near the strong surface vortex, the surface fluxes should be changed, which in turn should modify the heat and the moisture available for convection. On the wave side (see LMDW), this case was very interesting due to extreme sea states observed by the Canadian buoy array and the cruise ship *Queen Elizabeth II* (Bigio 1996).

b. Results

Figure 12 shows the track and central pressure of Hurricane Luis according to the National Hurricane Center and according to the simulations at 50- and 25-km resolutions. The simulations are far from the estimated central pressure values. The model trajectories are located too far west but this is partly improved in the higher-resolution run. While the 50-km simulation adopts a track more parallel to the real hurricane, the 25-km run results in a more irregular track and greater intensification in the last 12 hours, leading to higher wind speeds for the higher-resolution run. It is noteworthy that the model hurricane has an average speed of 18 m s^{-1} . With an intense and fast moving mesoscale system such as a hurricane, one can see the importance of a shorter coupling interval. With a coupling interval longer than $\frac{1}{2}$ h, the lag between the sea state and the wind field would become significant.

Figure 13 shows the 10-m wind speed difference between the WS and CH simulations, at a resolution of 25 km using a Kuo-type convection scheme, superimposed with the CH pressure pattern and its wind field. No significant change in the pressure pattern and the pressure center value was noted between the simulations. The expected reduction in the wind speed is noticed, but now there is also an increase of about 20% of the wind speed southwest of the system. This latter point is further discussed in LMDW.

Figure 14 shows the difference of the latent heat flux between the WS and the CH simulations superimposed with the WS precipitation rate and surface roughness length. The difference in the precipitation rate turns out to be very small. One of the reasons is that the location of maximum precipitation does not coincide with the regions where the largest impact of the coupling occurs. The largest difference in the vapor flux, corresponding to an increase of about 30% with respect to the uncoupled flux, also does not coincide with the region where the surface roughness length is large. In fact, the CH roughness length pattern (not shown) has a similar shape to that of WS, but with a maximum value of 4 mm. The results indicate that, for this case, the coupling does not have a strong impact on convection.

8. Summary and conclusions

The present work extends the results of previous studies of coupled atmospheric ocean wave model systems. Four real cases having different evolution or different mechanisms of development are simulated, covering a wide spectrum of meteorological conditions in the midlatitudes, and are used to assess the sensitivity of the coupling on the atmospheric response in a short-term perspective. The results from the four cases indicate that the most significant impact of the coupling is found in the 10-m wind speeds, where a reduction of about 10% occurs in association with enhanced surface roughness lengths due to the presence of younger and rougher seas.

Younger waves are generated where “fresh” winds are present (i.e., on the wave aspect, region where winds have not blown for a long duration and fetch in this direction). Such criteria are encountered along the coast when winds blow offshore and form new waves, at the leading edge of an advancing or developing storm, and over regions where a rapid shift in the wind direction is observed, such as, for example, near surface troughs or fronts. Changes in the vicinity of surface fronts can modulate the surface convergence and enhance locally the precipitation, but this does not necessarily play a crucial role in the rapid development of the storm. A critical factor for air–sea interaction and the subsequent development of the storm is the presence of a low-level jet. However, sensitivity tests with the case of February 1995 in which the coupling is multiplied by 5 over the surface jet reveals that, even with such exaggerated surface roughness, the impact of the coupling is relatively small overall. Therefore, the expected impact on the atmosphere with a realistic coupling, at the surface and in the vertical structure of the storm, appears to be negligible.

The better representation of the roughness length caused by the offshore winds blowing behind the storm and pushing cold air over warmer water increases the sensible and latent heat fluxes by a large percentage as well as increasing the friction velocity in a more modest proportion. The coupling modifies by about 30% the sea fluxes. However, these significant modifications in the fluxes create only very local changes and, thus, have a minor impact on the evolution of the storm. Moreover, these large changes in the fluxes are not located in active regions of the storm. Those changes result in a slight increase of the convective precipitation rate behind the system.

Wind speed comparisons between buoy observations and numerical simulations have to be interpreted cautiously because of the uncertain behavior of the buoys in high sea conditions, as discussed in [section 4b](#). However, marine forecasters and wave modelers generally agree that numerical models often overestimate the winds in stable conditions and underestimate them in unstable situations. The coupling would then decrease the overprediction of the wind speed found in stable conditions but would unfortunately accentuate the underprediction in the unstable cases. Thus, if the numerical simulation underpredicts the surface winds, as was the case for Luis, the coupling would cause a further deterioration of the surface wind forecast.

This study focuses on the impact of coupling on short-term forecasts of real cases of developing systems. The results indicate that the effects of coupling on the evolution and synoptic-scale aspects of the storm are rather weak, while small beneficial effects are noted on surface parameters. The study also demonstrates that the present generation of atmospheric mesoscale models does not need to know precisely the sea state, at such resolution, in order to produce reasonably accurate short-term forecasts. Knowledge of the sea state certainly does not deteriorate the forecasts, but the main impact is to enhance locally certain features of the storm. Such two-way interactions between an atmospheric and a wave model seems to show a stronger impact in a longer term perspective, as the [Janssen \(1994\)](#) study indicates.

Considering the small overhead in an operational context (about 1% CPU more time), where the wave model is run anyway using the meteorological model wind forecasts as a driver, then it might be worthwhile to consider running the coupled system. Small benefits can be expected on the atmospheric model, as shown here. The question of whether the coupling improves the wave forecast is discussed in Part II of this paper (see LMDW).

Acknowledgments

The work of the first author has been supported in part by the federal Panel on Energy Research and Development through the Ocean–Atmosphere Coupling Project and the Atmospheric Environment Service. Thanks are due to M. Desgagné, V. Lee, P. Pellerin, B. Bilodeau, and M. Valin for their assistance in running the MC2 model and in the development of the interface module for the coupling. Data from Canadian and American buoys were, respectively, supplied by B. Thomas and the National Buoy Center. This work benefited from useful discussions with W. Perrie and B. Toulany in the early stages. The lasting support of J. Abraham and P. Dubreuil throughout the project is gratefully acknowledged as well as useful comments by two anonymous reviewers.

REFERENCES

Benoit, R., J. Côté, and J. Mailhot, 1989: Inclusion of a TKE boundary layer parameterization in the Canadian regional finite element model. *Mon. Wea. Rev.*, **117**, 1726–1750.. [Find this article online](#)

—, M. Desgagné, P. Pellerin, S. Pellerin, Y. Chartier, and S. Desjardins, 1997: The Canadian MC2: A semi-Lagrangian, semi-implicit wide band atmospheric model suited for fine-scale process studies and simulation. *Mon. Wea. Rev.*, **125**, 1726–1750.. [Find this article online](#)

Bigio, R., 1996: Significant and extreme waves generated by Hurricane Luis as observed by Canadian meteorological buoys and the Cunard cruise ship *Queen Elizabeth II*. *Can. Meteor. Oceanogr. Soc. Bull.*, **24**, 112–117..

Cardone, V. J., R. E. Jensen, D. T. Resio, V. R. Swail, and A. T. Cox, 1996: Evaluation of contemporary ocean wave models in rare extreme events: “Halloween Storm” of October 1991; “Storm of the Century” of March 1993. *J. Atmos. Oceanic Technol.*, **13**, 198–230..

Chalikov, D. V., and V. K. Makin, 1991: Models of the wave boundary layer. *Bound.-Layer Meteor.*, **56**, 83–99..

Charnock, H., 1955: Wind stress on a water surface. *Quart. J. Roy. Meteor. Soc.*, **81**, 639–640..

Chouinard, C., J. Mailhot, H. Mitchell, A. Staniforth, and R. Hogue, 1994: The Canadian regional data assimilation system: Operational and research applications. *Mon. Wea. Rev.*, **122**, 1306–1325..

Desjardins, S., R. Benoit, and V. Swail, 1998: The influence of mesoscale features of the sea surface temperature distribution on marine boundary layer winds off the scotian shelf during the superstorm of March 1993. *Mon. Wea. Rev.*, **126**, 2793–2808.. [Find this article online](#)

Donelan, M. A., 1982: The dependence of the aerodynamic drag coefficient on wave parameters. *Proc. First Int. Conf. on Meteorology and Air–Sea Interaction of the Coastal Zone*, The Hague, Netherlands, Amer. Meteor. Soc., 381–387..

Doyle, J. D., 1995: Coupled ocean wave/atmosphere mesoscale model simulations of cyclogenesis. *Tellus*, **47A**, 766–778..

— and T. T. Warner, 1993: A three-dimensional numerical investigation of a Carolina coastal low-level jet during GALE IOP 2. *Mon. Wea. Rev.*, **121**, 1030–1047.. [Find this article online](#)

Huo, S., D. L. Zhang, J. Gyakum, and A. Staniforth, 1995: A diagnostic analysis of the superstorm of March 1993. *Mon. Wea. Rev.*, **123**, 1740–1761.. [Find this article online](#)

Kocin, J. P., P. N. Schumacher, R. F. Morales Jr., and L. Uccellini, 1995: Overview of the 12–14 March 1993 Superstorm. *Bull. Amer. Meteor. Soc.*, **76**, 165–182.. [Find this article online](#)

Komen, G. J., R. J. Reed, and S. Low-Nam, 1991: Effects of surface energy fluxes during the early development and rapid intensification stages of seven explosive cyclones in the western Atlantic. *Mon. Wea. Rev.*, **119**, 457–476.. [Find this article online](#)

—, L. Cavaleri, M. Donelan, M. Hasselmann, K. Hasselmann, and P. A. E. M. Janssen, 1994: *Dynamics and Modelling of Ocean Waves*. Cambridge University Press, 532 pp..

Kuo, Y.-H., 1974: Further studies on the parameterization of the influence of cumulus convection on large-scale flow. *J. Atmos. Sci.*, **31**, 1232–1240.. [Find this article online](#)

Janssen, P. A. E. M., 1989: Wave-induced stress and the drag of air flow over sea waves. *J. Phys. Oceanogr.*, **19**, 745–754.. [Find this article online](#)

—, 1991: Quasi-linear theory for wind-wave generation applied to wave forecasting. *J. Phys. Oceanogr.*, **21**, 1631–1642.. [Find this article online](#)

—, 1994: Results with a coupled wind wave model: ECMWF Tech. Rep. No. 71, 60 pp. [Available from ECMWF, Shinfield Park, Reading RG2 9AX, United Kingdom.].

— and P. Viterbo, 1996: Ocean waves and the atmospheric climate. *J. Climate*, **9**, 1269–1287.. [Find this article online](#)

—, A. C. M. Beljaars, A. Simmons, and P. Viterbo, 1992: The determination of surface stress in an atmospheric model. *Mon. Wea. Rev.*, **120**, 2977–2985.. [Find this article online](#)

Lalbeharry, R., J. Mailhot, S. Desjardins, and L. Wilson, 2000: Examination of the impact of a coupled atmospheric and ocean wave system. Part II: Ocean wave aspects. *J. Phys. Oceanogr.*, **30**, 402–415.. [Find this article online](#)

Lapenta, W. M., and N. L. Seaman, 1992: A numerical investigation of East Coast cyclogenesis during the cold-air damming event of 27–28 February 1982. Part II: Importance of physical mechanisms. *Mon. Wea. Rev.*, **120**, 52–76.. [Find this article online](#)

Lionello, P., P. Malguzzi, and A. Buzzi, 1998: Coupling between the atmospheric circulation and ocean wave field: An idealized case. *J. Phys. Oceanogr.*, **28**, 161–177.. [Find this article online](#)

Maat, N., C. Kraan, and W. A. Oost, 1991: The roughness of waves. *Bound.-Layer Meteor.*, **54**, 89–103..

Mailhot, J., and C. Chouinard, 1989: Numerical forecast of explosive winter storms: Sensitivity experiments with a meso- α model. *Mon. Wea. Rev.*, **117**, 1311–1343.. [Find this article online](#)

—, —, R. Benoit, M. Roch, G. Verner, J. Côté, and J. Pudykiewicz, 1989: Numerical forecasting of winter coastal storms during CASP: Evaluation of the regional finite-element model. *Atmos.–Ocean*, **27**, 27–58..

- R. Sarrazin, B. Bilodeau, N. Brunet, and G. Pellerin, 1997: Development of the 35-km version of the Canadian regional forecast system. *Atmos.–Ocean*, **35**, 1–28.
- S. Bélair, R. Benoit, B. Bilodeau, Y. Delage, L. Fillion, L. Garand, C. Girard, and A. Tremblay, 1998: Scientific description of RPN Physics Library—Version 3.6, 188 pp. [Available from RPN, 2121 Trans-Canada, Dorval, QC H9P 1J3, Canada.]
- Makin, V. K., and C. Mastenbroek, 1996: Impact of waves on air–sea exchange of sensible heat and momentum. *Bound.-Layer Meteor.*, **79**, 279–300.
- Pond, S., 1968: Some effect of buoy motion on measurement of wind speed and stress. *J. Geophys. Res.*, **73** (2), 507–512.
- Reed, R. J., G. A. Grell, and Y.-H. Kuo, 1993: The ERICA IOP 5 storm. Part II: Sensitivity tests and further diagnosis based on model output. *Mon. Wea. Rev.*, **121**, 1595–1612. [Find this article online](#)
- Skey, S. G. P., K. Berger-North, and V. R. Swail, 1995: Detailed measurement of winds and waves in high sea states from a moored NOMAD weather buoy. *Proc. Fourth. Int. Workshop on Wave Hindcasting and Forecasting*, Banff, AB, Canada, Federal Panel on Energy R & D, 213–223.
- — and — —, 1998: Measurement of winds and waves from a NOMAD buoy in high sea states. *Proc. Fifth Int. Workshop on Wave Hindcasting and Forecasting*, Melbourne, FL, Federal Panel on Energy R & D, 163–175.
- Smith, S. D., 1981: Factors for adjustment of wind speed over water to a 10 metre height. Report Series/BI-R-81-3/March 81, Bedford Institute of Oceanography, Bedford, NS, Canada, 29 pp. [Available from BIO, P.O. Box 1006, Dartmouth, NS B2Y 4A2, Canada.]
- —, 1988: Coefficients for sea surface wind stress, heat flux and wind profiles as a function of wind speed and temperature. *J. Geophys. Res.*, **93**, 15 467–15 472.
- —, 1989: Water vapour flux at the sea surface. *Bound.-Layer Meteor.*, **47**, 277–293.
- — and Coauthors, 1992: Sea surface wind stress and drag coefficients: The HEXOS results. *Bound.-Layer Meteor.*, **60**, 109–142.
- Tanguay, M., A. Robert, and R. Laprise, 1990: A semi-implicit semi-Lagrangian fully compressible regional forecast model. *Mon. Wea. Rev.*, **118**, 1970–1980. [Find this article online](#)
- Uccellini, L. W., R. A. Petersen, K. F. Brill, P. J. Kocin, and J. J. Tuccillo, 1987: Synergetic interactions between and upper-level jet streak and diabatic processes that influence the development of a low-level jet and a secondary coastal cyclone. *Mon. Wea. Rev.*, **115**, 2227–2261. [Find this article online](#)
- WAMDI Group, 1988: The WAM model—A third generation ocean wave prediction model. *J. Phys. Oceanogr.*, **18**, 1775–1810. [Find this article online](#)
- Weber, S., H. von Storch, P. Viterbo, and L. Zambresky, 1993: Coupling an ocean wave to an atmospheric general circulation model. *Climate Dyn.*, **9**, 63–69.
- Wu, J., 1980: Wind stress coefficients over the sea surface during near neutral conditions—A revisit. *J. Phys. Oceanogr.*, **10**, 727–740. [Find this article online](#)
- Yau, M. K., and M. Jean, 1989: Synoptic aspects and physical processes in the rapidly-intensifying cyclone of 6–8 March 1986. *Atmos.–Ocean*, **27**, 59–86.
- Zika, M., and P. J. Kocin, 1998: Mesoscale aspects of northeast snowstorms. *Preprints, 16th Conf. Weather Analysis and Forecasting*. Phoenix, AZ, Amer. Meteor. Soc., 418–420.

APPENDIX

9. Simplified Scale Analysis

One can derive simple equations that express the changes, due to the coupling, of the surface roughness length, the wind speed, and the fluxes in terms of change in the friction velocity and the sea state. One assumes, for the sake of simplicity, neutral conditions. The reference height $z = 10$ m and the von Kármán constant $\kappa = 0.41$.

a. Roughness length

Starting from the Charnock relation with β as the Charnock parameter,

$$z_0 = \frac{\beta}{g} u_*^2. \quad (\text{A1})$$

Applying the logarithm on (A1) and deriving this last expression, one can easily find

$$\left(\frac{\Delta z_0}{z_0} \right) = 2 \left(\frac{\Delta u_*}{u_*} \right) + \left(\frac{\Delta \beta}{\beta} \right), \quad (\text{A2})$$

where the ratio $\Delta x/x$ is given as {coupled x – uncoupled x }/uncoupled x and uncoupled refers to the control run.

b. 10-m wind speed

Starting from the neutral log wind profile equation in which z is a reference height

$$u_z = \frac{u_*}{\kappa} \ln \frac{z}{z_0} \quad (\text{A3})$$

and by deriving this equation, one obtains

$$\Delta u_z = \frac{\Delta u_*}{\kappa} \ln \frac{z}{z_0} - \frac{u_*}{\kappa} \frac{\Delta z}{z_0}. \quad (\text{A4})$$

Using (A2) and (A3), one can easily change the last expression to

$$\Delta u_z = \frac{u_z}{u_*} \Delta u_* - \frac{u_*}{\kappa} \left[2 \frac{\Delta u_*}{u_*} + \frac{\Delta \beta}{\beta} \right]. \quad (\text{A5})$$

Dividing (A5) by u_z and after rearranging terms, one finally finds as we replace the reference height z by its value:

$$\left(\frac{\Delta u_{10}}{u_{10}} \right) = \left[1 - 2 \frac{u_*}{\kappa u_{10}} \right] \left(\frac{\Delta u_*}{u_*} \right) - \frac{u_*}{\kappa u_{10}} \left(\frac{\Delta \beta}{\beta} \right), \quad (\text{A6})$$

the general form of the variation of the 10-m wind speed.

Defining the neutral drag coefficient, with the help of (A3), as

$$C_D \equiv \frac{u_*^2}{u_{10}^2} = \frac{\kappa^2}{\left[\ln \left(\frac{z}{z_0} \right) \right]^2}, \quad (\text{A7})$$

one finds

$$\left(\frac{\Delta C_D}{C_D} \right) = 2 \frac{\sqrt{C_D}}{\kappa} \left(\frac{\Delta z_0}{z_0} \right). \quad (\text{A8})$$

Applying (A7) in (A6), one obtains

$$\left(\frac{\Delta u_{10}}{u_{10}}\right) = \left[1 - 2\frac{\sqrt{C_D}}{\kappa}\right]\left(\frac{\Delta u_*}{u_*}\right) - \frac{\sqrt{C_D}}{\kappa}\left(\frac{\Delta\beta}{\beta}\right). \quad (\text{A9})$$

If one assumes, in a range of high wind speeds, a mean drag coefficient = 2.5×10^{-3} , [Eq. \(A6\)](#) simplifies to

$$\left(\frac{\Delta u_{10}}{u_{10}}\right) = 0.76\left(\frac{\Delta u_*}{u_*}\right) - 0.12\left(\frac{\Delta\beta}{\beta}\right). \quad (\text{A10})$$

c. Surface fluxes

Taking as a general form the following equation to express surface heat or moisture fluxes:

$$F_\zeta = \rho C_\zeta \Delta \zeta (u_z C_H), (\text{A11})$$

where ζ represents the variable of the flux treated, Δ represents the variation between the surface and the reference height z of the usual variable defining the flux, and C_ζ is the related constant. For example, in term of latent heat flux, C_ζ is the latent heat of evaporation and the variation is for humidity. Let us assume that this latter variation is not affected by the coupling.

In [\(A11\)](#), C_H is the heat (moisture) flux coefficient, or the Stanton number, defined as

$$C_H = \frac{\kappa}{\text{Pr}} \frac{C_D^{1/2}}{\ln\left(\frac{z}{z_{0T}}\right)}, \quad (\text{A12})$$

and where Pr is the turbulent Prandtl number (=const), z_{0T} is the roughness length for heat (or moisture), and C_D is the neutral drag coefficient defined in [\(A7\)](#).

Three cases are considered here:

1) Constant Stanton number (cf. [Makin and Mastenbroek 1996](#))

It can be easily shown by deriving [\(A11\)](#) that

$$\left.\frac{\Delta F_\zeta}{F_\zeta}\right|_{C_H=\text{cte}} = \frac{\Delta u_z}{u_z} = (\text{A9}). \quad (\text{A13})$$

2) Constant Z_{0T} (cf. [Makin and Mastenbroek 1996](#))

This means from [\(A12\)](#) that $C_H \propto C_D^{1/2}$. By deriving [\(A11\)](#), one finds that

$$\left.\frac{\Delta F_\zeta}{F_\zeta}\right|_{Z_{0T}=\text{cte}} = \frac{1}{2} \frac{\Delta C_D}{C_D} + \frac{\Delta u_z}{u_z}, \quad (\text{A14})$$

and using [\(A8\)](#), [\(A9\)](#), and [\(A2\)](#), the expression becomes

$$\left.\frac{\Delta F_\zeta}{F_\zeta}\right|_{Z_{0T}=\text{cte}} = \frac{\Delta u_*}{u_*}. \quad (\text{A15})$$

3) $Z_{0T} = Z_0$ (i.e., full sea state dependency)

This means from (A12) and (A7) that $C_H = (1/Pr) \cdot C_D$. By deriving (A11), one finds that

$$\left. \frac{\Delta F_\zeta}{F_\zeta} \right|_{Z_{0T}=Z_0} = \frac{\Delta C_D}{C_D} + \frac{\Delta u_z}{u_z}, \quad (\text{A16})$$

and using (A8), (A9), and (A2), the expression becomes

$$\left. \frac{\Delta F_\zeta}{F_\zeta} \right|_{Z_{0T}=Z_0} = \left[1 + \frac{2\sqrt{C_D}}{\kappa} \right] \left(\frac{\Delta u_*}{u_*} \right) + \frac{\sqrt{C_D}}{\kappa} \left(\frac{\Delta \beta}{\beta} \right). \quad (\text{A17})$$

Finally, if one assumes a mean drag coefficient = 2.5×10^{-3} Eq. (A17) simplifies to

$$\frac{\Delta F_\zeta}{F_\zeta} = 1.24 \left(\frac{\Delta u_*}{u_*} \right) + 0.12 \left(\frac{\Delta \beta}{\beta} \right). \quad (\text{A18})$$

Tables

Table 1. Time frame of each case for the specific phases of the simulation strategy.

Case	Date	Spinup 1 (date/UTC)	Spinup 2 (date/UTC)	Transition (date/UTC)	Evaluation (date/UTC)
1	Mar 1993	11:00-12:00	12:00-13:00	13:00-14:00	14:00-16:00
2	Mar 1998	01:12-04:12	04:12-05:12	05:12-06:12	06:12-08:12
3	Feb 1995	01:00-02:00	02:00-03:00	03:00-04:00	04:00-06:00
4	Sep 1995	07:00-08:00	08:00-09:00	09:00-10:00	10:00-11:12

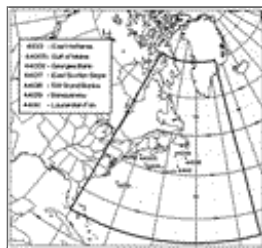
[Click on thumbnail for full-sized image.](#)

Table 2. List of experiments according to the case study.

Case	Spinup 1	Spinup 2	Transition	Evaluation
1	CH/(WS)	CH/(WS)	CH/(WS) WS WA	CH/(WS) WS WA
2	CH/(WS)	CH/(WS)	CH/(WS) WS	CH/(WS) WS
3	CH/(WS)	CH/(WS)	CH/(WS) WS 5WS	CH/(WS) WS 5WS
4	CH/(WS)	CH/(WS)	CH/(WS) WS	CH/(WS) WS

[Click on thumbnail for full-sized image.](#)

Figures



[Click on thumbnail for full-sized image.](#)

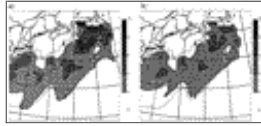
Fig. 1. MC2 grid used. The wave model grid is enclosed with the darker lines. Locations and names of the buoys used are indicated.





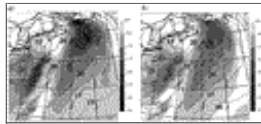
[Click on thumbnail for full-sized image.](#)

Fig. 2. Six-hour observed trajectory and pressure center values for the four storms. Starting date of each trajectory is indicated in the corner.



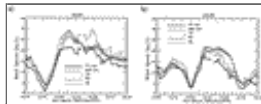
[Click on thumbnail for full-sized image.](#)

Fig. 3. The 12-h surface roughness length (10^{-3} m) forecast valid at 1200 UTC 14 March 1993 from coupled (grayscale) and uncoupled CH (dashed and labeled) runs for (a) WS and (b) WA.



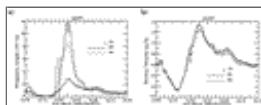
[Click on thumbnail for full-sized image.](#)

Fig. 4. The 12-h forecast valid at 1200 UTC 14 March 1993 of the 10-m wind speed difference (m s^{-1} , grayscale) between coupled and uncoupled simulations and the coupled wind field (dashed and labeled) for (a) WS and (b) WA.



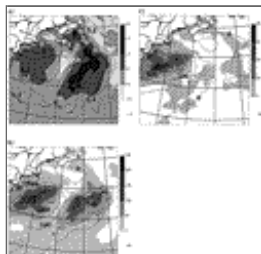
[Click on thumbnail for full-sized image.](#)

Fig. 5. Times series of 10-m wind speed for the (a) East Scotian Slope (44137) and (b) Banquereau (44138) buoys for the period of 13–16 March 1993. The results from CH, WS, and WA runs are shown with the observed 10-min averaged and maximum wind speeds.



[Click on thumbnail for full-sized image.](#)

Fig. 6. Times series at the location of the East Scotian Slope (44137) buoy for (a) surface roughness length and (b) friction velocity for CH, WS, and WA runs.



[Click on thumbnail for full-sized image.](#)

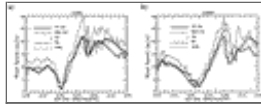
Fig. 7. Difference of surface fields (grayscale) between a coupled run (WS) and the control run (CH) superimposed with the coupled field (dashed and labeled). (a) Friction velocity (0.1 m s^{-1}), (b) sensible heat flux (W m^{-2}), and (c) latent heat flux (W m^{-2}). The 24-h forecast valid at 1200 UTC 7 March 1986. Coupled 10-m wind field (m s^{-1}) is superimposed in (a).





[Click on thumbnail for full-sized image.](#)

Fig. 8. The 24-h total precipitation rate (2 mm h^{-1}) forecast valid at 1200 UTC 7 March 1986 for WS (grayscale) and CH (dashed lines).



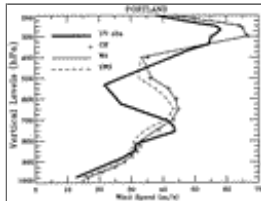
[Click on thumbnail for full-sized image.](#)

Fig. 9. Time series of 10-m wind speed for the (a) East Hatteras (41001) and (b) Gulf of Maine (44005) buoys. CH, WS, and 5WS refer to the uncoupled, the wave-induced stress, and the “boosted” simulations, respectively.



[Click on thumbnail for full-sized image.](#)

Fig. 10. The 24-h sea level pressure forecast valid at 0000 UTC 5 February 1995 and the 10-m wind field. Darker lines or wind barbs are for 5WS, while thinner wind barbs and dashed lines are for WS.



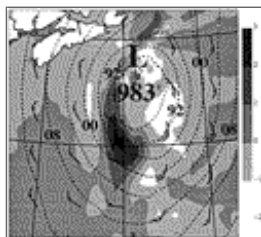
[Click on thumbnail for full-sized image.](#)

Fig. 11. Wind speed vertical profile at Portland, Maine, at 0000 UTC on 5 March 1995. For the definition of lines see legend in graph.



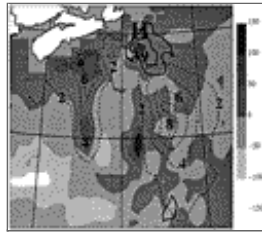
[Click on thumbnail for full-sized image.](#)

Fig. 12. Trajectory of observed and simulated Hurricane Luis from 0000 UTC 10 September to 0600 UTC 11 September 1995. Central pressure values are indicated.



[Click on thumbnail for full-sized image.](#)

Fig. 13. The 24-h forecast valid at 0000 UTC 11 September 1995 of the 10-m wind speed difference (1 m s^{-1} , grayscale) between coupled (WS) and uncoupled (CH) simulations superimposed with the WS wind field and the sea level pressure (dashed and labeled).



[Click on thumbnail for full-sized image.](#)

Fig. 14. The 24-h forecast valid at 0000 UTC 11 September 1995 of the difference of latent heat flux (grayscale, W m^{-2}) between the coupled run (WS) and the control run (CH) superimposed with the WS roughness length (10^{-3} m , dashed and labeled) and the WS total precipitation rate (10 mm h^{-1} , thick solid).

Corresponding author address: Serge Desjardins, Environment Canada, Atlantic Region, 16th floor, Queen Centre, 45 Alderney Drive, Dartmouth, NS B2Y 2N6, Canada.

E-mail: Serge.Desjardins@ec.gc.ca

[top ▲](#)



© 2008 American Meteorological Society [Privacy Policy and Disclaimer](#)
Headquarters: 45 Beacon Street Boston, MA 02108-3693
DC Office: 1120 G Street, NW, Suite 800 Washington DC, 20005-3826
amsinfo@ametsoc.org Phone: 617-227-2425 Fax: 617-742-8718
[Allen Press, Inc.](#) assists in the online publication of AMS journals.